Supporting Information for

Structural Plasticity as a Driver of the Maturation of Pro-Interleukin-18

Jeffrey P. Bonin[1,2,3,*], James M. Aramini[1], and Lewis E. Kay[1,2,3,*]

[1]Departments of Molecular Genetics and Biochemistry, University of Toronto, Toronto, Ontario, M5S 1A8, Canada

[2]Department of Chemistry, University of Toronto, Toronto, Ontario, M5S 3H6, Canada

[3]Program in Molecular Medicine, The Hospital for Sick Children Research Institute, Toronto, Ontario, M5G 0A4, Canada

Materials & Methods

Cloning, Expression, Purification, and Sample Preparation for NMR Studies

Isotopically enriched samples of pro-IL-18 were expressed and purified from *E. coli* using a previously established protocol [1]. Briefly, the 193-residue coding sequence of pro-IL-18 was cloned into the Champion pET SUMO vector (ThermoFisher Scientific) in frame with an N-terminal 6x His and SUMO tag, transformed into *Escherichia coli* BL21 (DE3) cells, and expressed in M9 minimal medium containing either *U*-$^{15}NH_4Cl$ and *U*-^{13}C-glucose as the sole nitrogen and carbon sources for the production of a *U*-[^{13}C,^{15}N] sample or *U*-$^{15}NH_4Cl$ and ^{12}C-glucose for generating [*U*-^{15}N]-pro-IL-18. For *U*-^{2}H samples with ILV $^{13}CH_3$-labeling (with only one of the prochiral methyl groups of Leu and Val $^{13}CH_3$ labeled in a non-stereospecific manner), cells were grown in M9 D_2O medium with *U*-$^{15}NH_4Cl$ and d_7-glucose, and precursors (60 mg/L

α-ketobutyric acid, methyl-$^{13}C\{3,3\text{-}D2\}$ for Ileδ1-$^{13}CH_3$; 100 mg/L α-ketoisovaleric acid, 3-methyl-$^{13}C\{3,4,4,4\text{-}D4\}$ for Leuδ, Valγ-$^{13}CH_3/^{12}CD_3$) were added to media 1 hour prior to the induction of protein expression. Initial cell growth was carried out at 37 °C, and protein expression was induced at 25 °C by 0.1 mM IPTG at an OD_{600} of 0.8 and continued for 20 hours. Protein purification was carried out at room temperature using 20 mM Tris buffers at pH 8. Cells were lysed by sonication on ice in the presence of 0.5 M NaCl and a trace of DNase I. Clarified cell extracts were loaded onto a NiNTA column, purified by a wash step with 10 mM imidazole, and then the 6x His labeled protein was eluted using 0.3 M imidazole. The 6x His and SUMO tags were then cleaved by Ulp protease during an overnight dialysis step to remove the imidazole, in the presence of 0.1 M NaCl. A second NiNTA step was performed in which the tag-less pro-IL-18 is found in the flow-through. Subsequently, pro-IL-18 was subjected to size exclusion chromatography using a prepacked 16/600 Superdex 75 column in the presence of 50 mM NaCl. The final yield of purified isotopically-enriched pro-IL-18 was approximately 22 mg/L of culture. Sample purity was confirmed by SDS-PAGE. Samples were concentrated by ultracentrifugation to ~0.5-1 mM (see Data Acquisition section below for concentrations of each sample) in 20 mM MES, 50 mM NaCl, and 10 mM DTT at pH 6.5, and 3% D_2O and 0.5 mM EDTA were added to each sample. In contrast, the sample for recording the hydrogen-deuterium exchange was lyophilized and resuspended in 20 mM MES, 50 mM NaCl, 10 mM DTT, and 0.5 mM EDTA in 99.8% D_2O and pD (corrected) was 5.85 [2].

NMR Spectroscopy

NMR experiments were collected at 40 °C (unless stated otherwise) on Bruker AVANCE NEO 23.5 T (1.0 GHz) and AVANCE III HD 18.8 T (800 MHz) and 14.1 T (600 MHz) NMR spectrometers equipped with 5-mm TCI triple-axis gradient cryoprobes. The recorded data were

processed with NMRPipe[3], visualized using NMRFAM-SPARKY[4], and peak intensities/volumes were fit using peakipy (https://github.com/j-brady/peakipy). Our previously reported resonance assignments for pro-IL-18 were used (BMRB ID 31122).

Data Acquisition

HSQC of P93T and WT pro-IL-18

Gradient-enhanced sensitivity 2D ^{1}H-^{15}N HSQC [5] spectra were recorded at 25 ^{o}C at 1 GHz (P93T) and 800 MHz (WT) on *U*-[^{15}N] samples. Sample concentrations were 0.2 mM (P93T) and 1.0 mM (WT).

^{15}N and methyl ^{1}H relaxation

^{15}N spin relaxation experiments were recorded on a 0.6 mM *U*-[^{2}H,^{15}N] ILV $^{13}CH_3$ sample at 800 MHz. Relaxation rates for the two-spin elements HxNx, HxNz, HzNx, HzNz [6], and ^{15}N $R_{1\rho}$ relaxation rates were recorded with 9 relaxation times (5, 10, 15, 20, 25, 30, 35, 40, 50 ms) using ^{15}N (HxNx, HzNx, and ^{15}N $R_{1\rho}$) and ^{1}H (HxNx, HxNz,) spin lock powers of 2 kHz and 12.5 kHz, respectively. ^{15}N R_1 relaxation rates were recorded with 5 relaxation times (10, 125, 250, 375, 500 ms) and a 2 kHz ^{15}N spin lock was applied far off-resonance for 50 ms during the interscan delay ensuring equivalent sample heating in the R_1 and $R_{1\rho}$ experiments. ^{15}N{^{1}H}-heteronuclear NOEs were recorded using a total interscan delay of 14 s. In the saturation experiment, 180^{o} ^{1}H pulses (6 dB lower power than the ^{1}H hard pulse) are applied with 22 ms spacings [7] for 6 of the 14 s. ^{15}N spin relaxation measurements were recorded with pulse sequences similar to those used in Farrow *et al.* [8], with the exception that a spin-lock element was used to measure $R_{1\rho}$ rates rather than refocused free-precession of magnetization from which R_2 rates are obtained.

Methyl ^{1}H-^{1}H cross-correlated relaxation rates [9], from which values of $S^2_{axis}\tau_c$ were calculated for each methyl group, were measured at 1 GHz using 12 relaxation times (2, 5, 8, 12, 17, 22, 27, 32, 37, 42, 50, 60 ms).

CPMG and CEST

^{15}N, ^{1}HN, and methyl experiments were recorded on *U*-[^{2}H,^{15}N] ILV $^{13}CH_3$ samples, while ^{13}CO, ^{13}Cα, ^{13}Cβ, and ^{1}Hα experiments were recorded on *U*-[^{13}C,^{15}N] samples. Spin lock carrier frequency sampling schedules for all CEST experiments were determined using an optimized frequency sampling approach [10]. All ^{1}H CEST experiments were of the class whereby longitudinal order (IzSz, where Iz and Sz are z-components of ^{1}H and S=^{15}N,^{13}C magnetization, respectively) is selected at the end of the relaxation period [11]. For CPMG experiments, two duplicate planes were collected for peak intensity error estimation. Relevant parameters regarding the acquisition of the CPMG and CEST datasets are given in Tables S1 and S2.

Hydrogen-deuterium exchange

U-[^{15}N] pro-IL-18 was lyophilized and resuspended in D_2O buffer at pD (corrected) of 5.85 (see Sample Preparation section above). Probe tuning, matching, and shimming were performed on a buffer-only sample prior to resuspension of the lyophilized protein, so that recording of spectra could begin immediately after injecting the protein sample into the spectrometer. Gradient-enhanced sensitivity 2D ^{1}H-^{15}N HSQC and proton 1D spectra were recorded at 800 MHz and 25 ^{o}C. A proton 1D spectrum was recorded after every HSQC dataset to monitor the intensity of the methyl signals, which do not undergo hydrogen-deuterium exchange over time, thus ensuring the fidelity of the sample. The duration of a single HSQC and proton 1D was 3.5 minutes. 139 (HSQC+1D) spectra were recorded in total, spanning a period of 2.8 days; 71 of these were recorded continuously, followed by 63 collected at 30 minute intervals, then one after 7 hours, and

four more collected at 5 hour intervals. At the end of the data collection, the methyl signal intensities had decreased by approximately 7% due to precipitation of the sample (amide signal intensities were corrected for this loss, see Analysis section below).

Data Analysis

^{15}N and methyl ^{1}H relaxation

The pure ^{15}N dipole-dipole transverse relaxation rate (i.e, not contaminated by chemical exchange), R_{dd}, of each amide was fit from the peak intensities obtained in the HxNx, HzNx, HxNz, and HzNz relaxation experiments using the following equation [6]:

$$\frac{1}{2}\ln\left(\frac{\tilde{I}_{HzNx}(t)\tilde{I}_{HxNz}(t)}{\tilde{I}_{HzNz}(t)\tilde{I}_{HxNx}(t)}\right) = -R_{dd}t$$

where $\tilde{I}_x(t)$ is the peak intensity from experiment x at time t relative to the corresponding intensity at time = 0 ms. The ^{15}N chemical exchange contribution to transverse relaxation under the spin lock conditions used, $R_{ex,\rho}$, of each amide was calculated using the following combination of relaxation rates [12]:

$$R_{ex,\rho} = \frac{1}{2}\left\{R_1(2HzNz)\left(-1+\frac{4c_N^2}{3d_{HN}^2}\right) + R_2(2HzNx)\left(1-\frac{4c_N^2}{3d_{HN}^2}\right)\right.$$
$$\left. + R_2(2HxNz)\left(-1-\frac{4c_N^2}{3d_{HN}^2}\right) + R_2(2HxNx)\left(1+\frac{4c_N^2}{3d_{HN}^2}\right)\right\}$$

where $R_y(x)$ is the relaxation rate for longitudinal order ($2HzNz; y=1$) or single ($2HzNx$, $2HxNz$; $y=2$) or multiple quantum ($2HxNx$; $y=2$) two spin elements, $c_N = B_0\gamma_N\Delta\sigma_N/\sqrt{3}$ ($\Delta\sigma_N = -163$ ppm used here), $d_{HN} = \left(\frac{\mu_0}{4\pi}\right)\hbar\gamma_H\gamma_N r_{HN}^{-3}$, B_0 is the static magnetic field strength, γ_x is the gyromagnetic ratio of nucleus x, $\Delta\sigma_N$ is the ^{15}N chemical shift anisotropy, μ_0 is the permeability of free space, $\hbar$ is Planck's constant divided by 2π, and r_{HN} is the vibrationally averaged distance between the ^{1}H and ^{15}N nuclei ($r_{HN} = 1.04$ Å used here).

^{15}N R_2 values were calculated from measured $R_{1\rho}$ relaxation rates as [13]

$$R_2 = \frac{R_{1\rho}}{\sin^2\theta} - \frac{R_1}{\tan^2\theta}\,.$$

where $\sin\theta = \frac{\omega_1}{\sqrt{\omega_1^2+\Omega^2}}$ and $\tan\theta = \frac{\omega_1}{\Omega}$, with ω_1 and Ω the spin-lock power and the offset of the ^{15}N spin in question from the ^{15}N carrier frequency, respectively.

Spectral density terms were calculated from these relaxation rates using the following equations [14]:

$$J(0.87\omega_H) = \frac{R_1 * NOE - R_1}{5\left(d_{HN}^2/4\right)(\gamma_H/\gamma_N)}$$

$$J(\omega_N) = \frac{R_1 - \left(7d_{HN}^2/4\right)(0.892)J(0.87\omega_H)}{\left(3d_{HN}^2/4\right) + c_N^2}$$

$$J(0)_{R_{1\rho}} = \frac{R_2 - \left((3d_{HN}^2/8) + \left(c_N^2/2\right)\right)J(\omega_N) - \left(13d_{HN}^2/8\right)(0.830)J(0.87\omega_H)}{\left(d_{HN}^2/2\right) + (2c_N^2/3)}$$

$$J(0)_{R_{2,corr}} = \frac{R_{2,corr} - \left((3d_{HN}^2/8) + \left(c_N^2/2\right)\right)J(\omega_N) - \left(13d_{HN}^2/8\right)(0.830)J(0.87\omega_H)}{\left(d_{HN}^2/2\right) + (2c_N^2/3)}$$

$$J(0)_{ex-free} = \frac{\left(\frac{8}{d_{HN}^2}\right)R_{dd} + 3J(\omega_N) - (0.845)J(0.87\omega_H)}{4}$$

where $J(x)$ is the spectral density function evaluated at frequency x, $J(0)_{R_{1\rho}}$ is the spectral density at zero frequency calculated using the R_2 obtained from $R_{1\rho}$, $J(0)_{R_{2,corr}}$ is the spectral density at zero frequency calculated using $R_{2,corr} = R_2 - R_{ex,\rho}$ (R_2 obtained from $R_{1\rho}$), and $J(0)_{ex-free}$ is the spectral density at zero frequency, uncontaminated by chemical exchange, calculated using R_{dd}.

The diffusion tensor was estimated from $R_{2,corr}$, R_1, and NOE rates of amides within the β strands ($n = 69$) using the ROTDIF software package [15], yielding a prolate axially symmetric diffusion tensor with rotational correlation time $\tau_c = \frac{1}{4D_\perp + 2D_\parallel} = 8.74 \pm 0.03$ ns, anisotropy $= \frac{D_\parallel}{D_\perp}$ $= 1.20 \pm 0.02$, $\alpha = 164 \pm 3°$, and $\beta = 133 \pm 3°$, where α and β are Euler angles relating the principal axis frame of the diffusion tensor to the molecular frame. Estimation of an axially symmetric diffusion tensor was repeated with the Modelfree software [16] using amides within β strands with NOE > 0.8 ($n = 52$), fixing $S_s^2 = 0.95$, $S_f^2 = 1.0$, and $\tau_s = 0$ ps. This yielded essentially identical values of $\tau_c = 8.78$ ns, anisotropy $= 1.25$, $\theta = 132.6°$, and $\varphi = 161.1°$. These parameters describing the diffusion tensor (Modelfree values) were then fixed in a dynamics analysis of all backbone amides for which relaxation rates could be quantified using Modelfree to determine S^2_s, S^2_f, and τ_s for each amide ($S^2 = S^2_s * S^2_f$). Note that R_{ex} was fixed at 0 for this analysis, since corrected transverse relaxation rates, $R_{2,corr} = R_2 - R_{ex,\rho}$, were used.

The methyl ^{1}H-^{1}H dipolar cross-correlated relaxation rate, η, is fit from the ratio of peak intensities resulting from forbidden (I_a(t)) and allowed (I_b(t)) transitions as a function of time, $\frac{I_a(t)}{I_b(t)}$, using the following equation [9]:

$$\frac{I_a(t)}{I_b(t)} = \frac{3}{4} \frac{\eta \tanh\left(\sqrt{\eta^2 + \delta^2}t\right)}{\sqrt{\eta^2 + \delta^2} - \delta \tanh\left(\sqrt{\eta^2 + \delta^2}t\right)}$$

where δ accounts for the coupling between rapidly and slowly decaying ^{1}H SQ coherences due to relaxation with external protons. Values of $S^2_{axis}\tau_c$ are then calculated from η using the relation:

$$\eta = \frac{9}{10}\left(\frac{\mu_0}{4\pi}\right)^2 [P_2(cos\theta_{axis,HH})]^2 \frac{S^2_{axis}\tau_c\gamma_H^4\hbar^2}{r^6_{HH}}$$

where μ_0 is the permeability of free space, $P_2(x) = \frac{1}{2}(3x^2 - 1)$, $\theta_{axis,HH}$ is the angle between the methyl 3-fold axis and a vector connecting a pair of methyl ^{1}H nuclei (90° used here), S^2_{axis} is the

order parameter describing the amplitude of motion of the methyl 3-fold axis, τ_c is the rotational correlation time (residue specific in this case due to anisotropic diffusion), γ_H is the gyromagnetic ratio of ^{1}H, $\hbar$ is Planck's constant divided by 2π, and r_{HH} is the distance between pairs of methyl protons (1.813 Å).

CPMG and CEST

All CPMG and CEST experiments were analyzed with the ChemEx program (https://github.com/gbouvignies/ChemEx). In all CPMG and CEST fits, R_2 values of nuclei in the ground and excited states were constrained to be equivalent. For the backbone probes (^{15}N, ^{1}HN, ^{13}CO), CPMG and CEST data for a given nucleus were analyzed together, that is, the same $\Delta\varpi$ and R_2 (at the same magnetic field) values were used for both. ^{15}N CPMG and CEST data from all exchanging residues ($\Delta R_2 \geq 2$ s^{-1} at 1 GHz) were fit to a linear 3-state model, as illustrated in Figure 4d ($k_{ex,AC}$ fixed at 0 s^{-1}). The resulting populations and exchange rates were then fixed in the analysis of the ^{1}HN data. For ^{13}CO, ^{13}Cα, ^{13}Cβ, and ^{1}Hα data, which were collected on protonated samples, slightly lower populations and exchange rates (see Table S9) were used (relative to values optimal for deuterated samples), based on a linear 3-state fit of ^{15}N CPMG data (1 GHz and 800 MHz) collected on a *U*-[^{15}N] sample in which $\Delta\varpi_{AB}$ and $\Delta\varpi_{AC}$ were fixed to the values obtained from the analysis on the deuterated sample.

For analysis of sidechain methyl groups, the ^{13}C CEST data were fit together with ^{13}C MQ CPMG and ^{1}H SQ CPMG datasets. ^{1}H CEST data were not included in the fit due to the influence of ^{1}H cross relaxation on the minor state populations extracted from these data [17]. However, in cases where a minor state dip is observed in the ^{1}H CEST profile, the $\Delta\varpi$ obtained from a 2-state fit of the ^{1}H CEST alone is fixed as $\Delta\varpi_{AC}$ in 3-state fits of the CPMG and ^{13}C CEST data (note that only state C is CEST visible). Otherwise, ^{1}H $\Delta\varpi_{AC}$ values are fit in the combined analysis of

the ^{13}C MQ CPMG, ^{1}H SQ CPMG and ^{13}C CEST data. For most of the methyl groups (19 of 25 methyls analyzed, Table S5), the populations and exchange rates were fixed to the values obtained in the backbone analysis. However, the methyl groups from residues in β1 (L45, V47, I48) were not fit well by this model (Figure S3). Instead, these methyl groups were fit together to a bifurcated 3-state model, with populations and exchange rates obtained from analysis of the methyl data with ^{1}H $\Delta\varpi_{AD}$ fixed as described above. In addition, V189γ_1 was also fit poorly by the backbone model, and was instead fit locally to a 3-state model with populations and exchange rates determined from the methyl data (see Table S9 for fit parameter values).

Hydrogen-deuterium exchange

Amide signal intensities were scaled by $\frac{methyl\ intensity(t_0)}{methyl\ intensity(t)}$ to compensate for signal loss due to the slight precipitation of the sample during the course of the experiment. The corrected amide intensities were then fit to a monoexponential decay function to determine the hydrogen exchange rate, k_{HDX}, of each amide. In the EX2 regime [18], which is applicable at the low pH and temperature conditions used here (pD_{corr} = 5.85, 25 ˚C), $k_{HDX} = p_{open} * k_{rc}$, where p_{open} is the population of the open (unfolded) state, and k_{rc} is the random coil hydrogen exchange rate under the conditions used [18]. The k_{rc} rates were estimated based on values from the laboratory of Englander [19–21], factoring in the corrected pD, temperature, and amino acid sequence. The free energy difference between open and closed states, ΔG, can then be calculated as:

$$\Delta G = -RTln(p_{open})$$

where R is the gas constant and T is the absolute temperature, assuming that p_{open} is small such that $p_{closed} \sim 1$ (i.e., the protein is very stable under the conditions of the experiment).

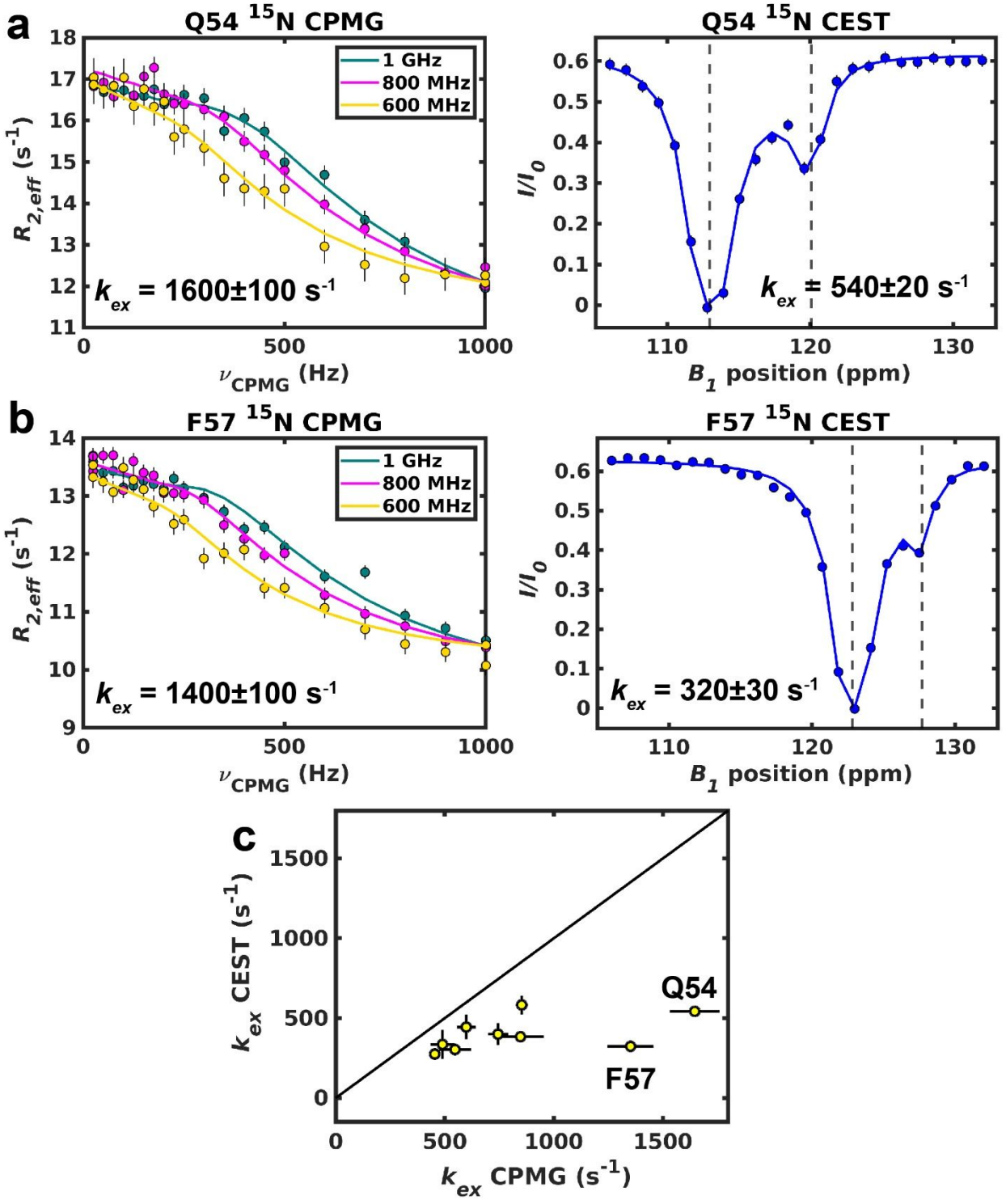

Figure S1: Residue specific 2-state fits of ^{15}N CPMG and CEST datasets yield distinct exchange rates, indicating that the exchange is more complex. (a) 2-state fit of ^{15}N CPMG data recorded at three static magnetic fields (1 GHz, 800 MHz, 600 MHz) for Q54 (left) and 2-state fit of ^{15}N CEST profiles recorded with two weak B_1 field strengths (44.3 and 19.2 Hz) (right). Only the 44.3 Hz dataset is shown in the CEST plot. Exchange rates, k_{ex}, obtained from independent

fits of CPMG and CEST data are shown in the plots and differ by about a factor of 3 for Q54. (b) Analogous plots are shown for F57. Exchange rates obtained differ by more than a factor of 4 for F57. (c) Correlation plot of exchange rates obtained from 2-state fits of ^{15}N CPMG and CEST datasets are shown for nine residues with pronounced minor state dips in CEST profiles. In all nine cases, the exchange rate obtained from the CPMG analysis exceeds that obtained via CEST, with most of the rates differing by ~1.4-2 fold for a given amide.

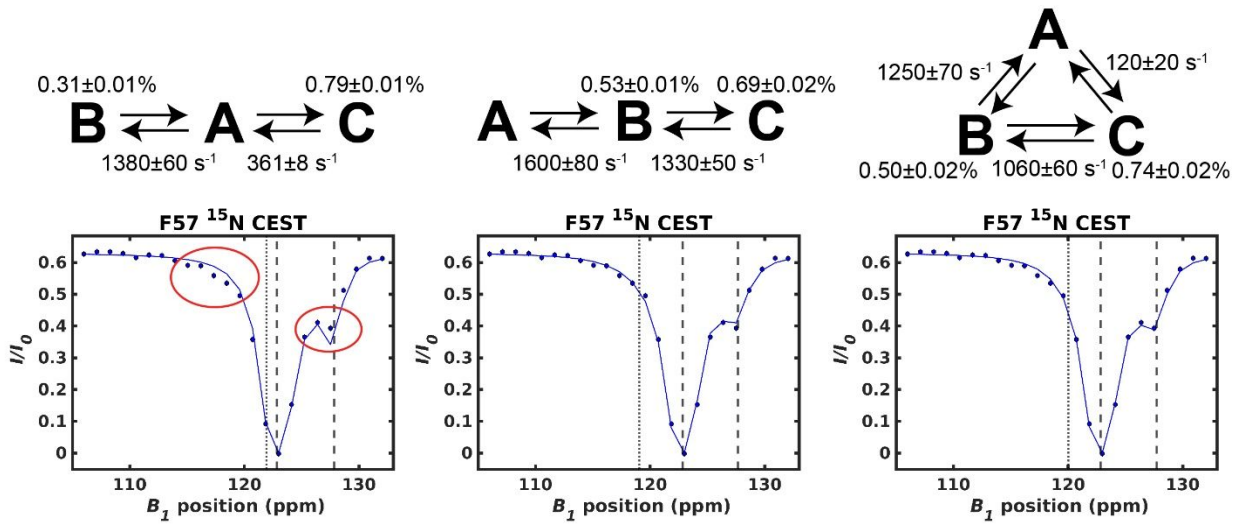

Figure S2: Comparison of various 3-state models establishes that the linear model (A↔B↔C) is the simplest which recapitulates the backbone relaxation data. ^{15}N CEST profiles (blue circles, 44.3 Hz weak B_1 field) are shown for F57 along with a fit (including ^{15}N CPMG and CEST data from all exchanging residues; solid line) using the 3-state model indicated above each CEST profile. Ground state (state A) and state C chemical shifts are indicated by the dashed lines, while the dotted line marks the chemical shift of state B. Regions where the fit from the bifurcated model (B↔A↔C) are poor, which coincide with the excited state chemical shifts obtained from the linear and triangular models, are marked by the red ovals. The fits from the linear and triangular models are in better agreement with experimental data in these regions. The populations and exchange rates obtained from the linear and triangular models are similar, and $\chi^2_{red} = 0.8$ for both models. Thus, we have used the simpler linear model to analyze the backbone CPMG and CEST data.

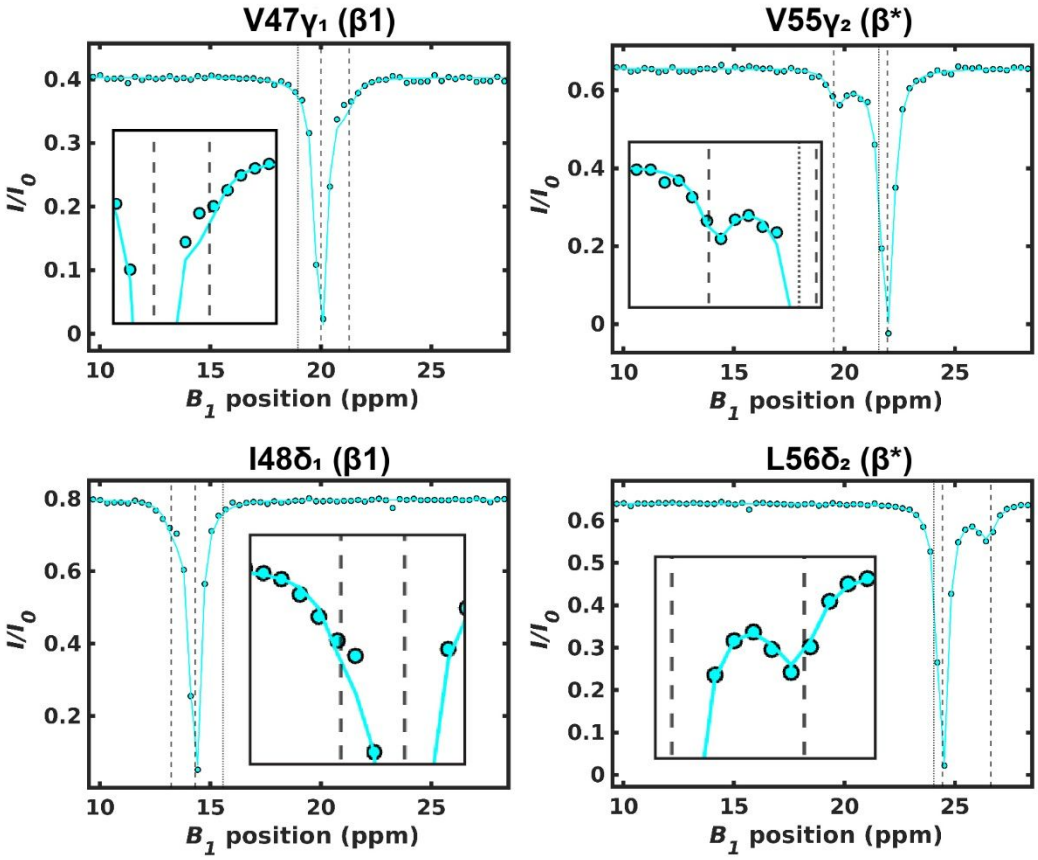

Figure S3: Global backbone exchange model describes ^{13}C CEST data of β* methyl groups well, but not those in β1. Methyl ^{13}C CEST profiles are shown for four methyl groups, two from β1 (V47γ_1 and I48δ_1) and two from β* (V55γ_2 and L56δ_2). Overlaid on the profiles are 3-state fits to the CEST data only, in which the populations and exchange rates were fixed to the values obtained from the analysis of the backbone data. Insets show the region around the minor state dip. While fits using the backbone model recapitulate the data from the methyl groups in β* very well, noticeable discrepancies in fits are seen for residues in β1, indicating that the μs-ms dynamics of the sidechain methyl groups of β1 are distinct from those in β*.

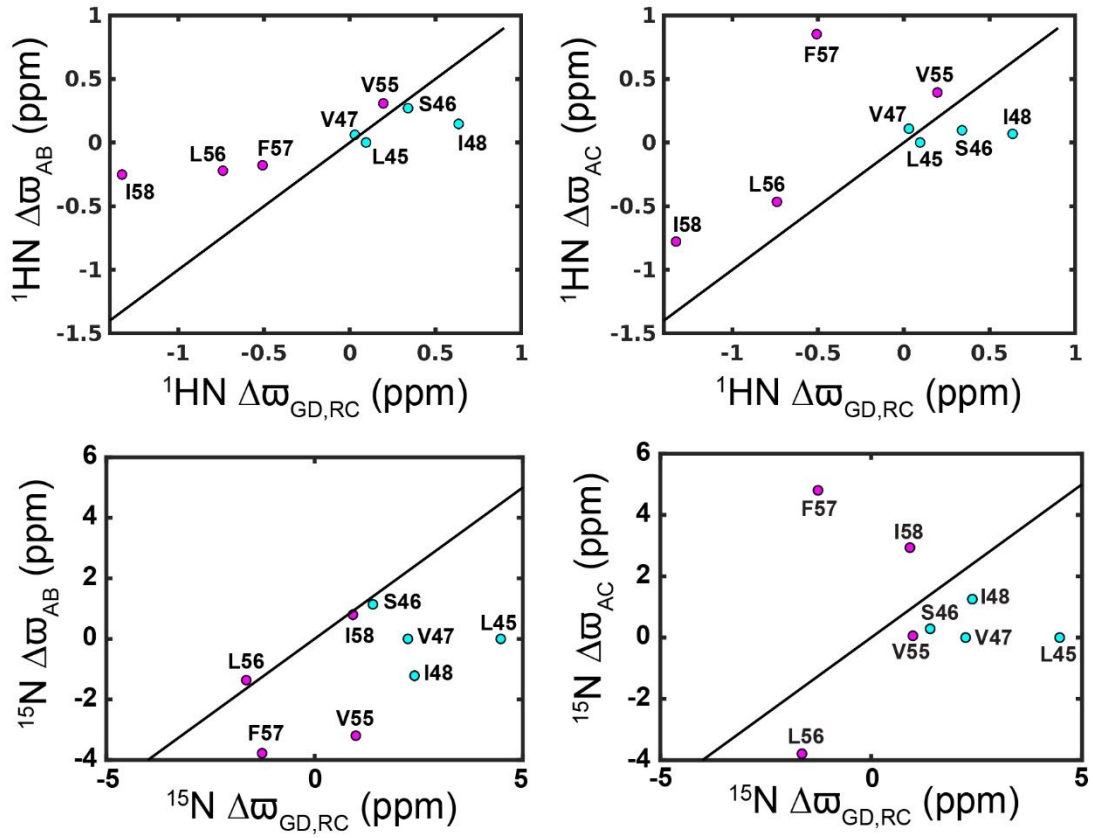

Figure S4: ^{1}HN and ^{15}N excited state chemical shifts of β1 and β* show poor agreement with predicted random coil shifts. ^{1}HN/^{15}N chemical shift differences between ground and excited states, $\Delta\varpi_{AB}$ and $\Delta\varpi_{AC}$, and ^{1}HN/^{15}N chemical shift differences between the ground state and random coil values, $\Delta\varpi_{GD,RC}$, are compared. Random coil chemical shifts were predicted using the method of Poulsen [22–25]. Amides from β1 and from β* are shown in cyan and in magenta, respectively. While some amide excited state shifts are in reasonable agreement with random coil chemical shift values, there are amides from both β1 and β* which have very poor agreement (for example, state B ^{1}HN: I48 from β1, I58 from β*, state C ^{1}HN: I48 from β1, F57 from β*). This suggests that neither β1 nor β* is unfolded in these excited states, consistent with our analysis based on all the backbone chemical shifts.

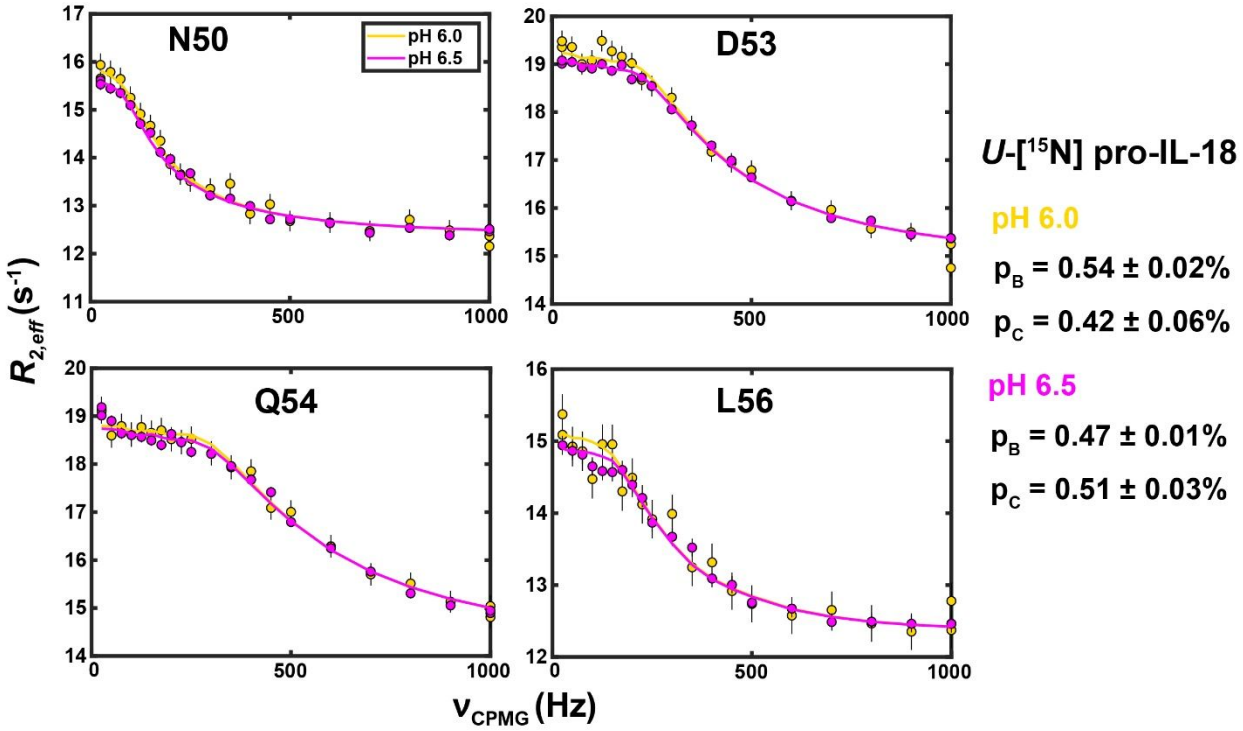

Figure S5: Populations of excited states detected by CPMG and CEST show little dependence on pH over a range from 6 to 6.5. ^{15}N CPMG profiles recorded at pH 6.5 (magenta) and 6.0 (gold) using *U*-[^{15}N] samples at 800 MHz are shown for several amides. Curves from a linear (A↔B↔C) 3-state fit, where $\Delta\varpi_{AB}$ and $\Delta\varpi_{AC}$ are fixed at the values obtained from the ^{15}N analysis of the *U*-[^{2}H,^{15}N] ILV $^{13}CH_3$ sample, are overlaid. The resulting populations are shown; these are similar between pH 6.0 and 6.5.

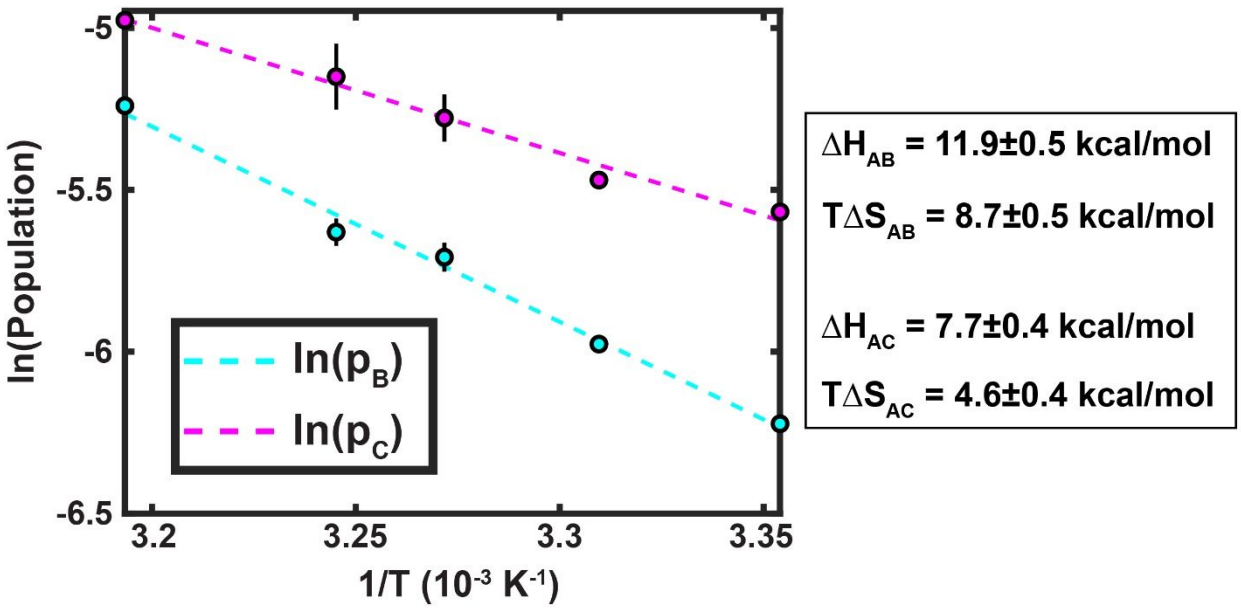

Figure S6: Temperature dependence of excited state populations indicate enthalpically unfavorable and entropically favorable transitions to the excited states. Plots of ln(Population) as a function of 1/T are linear for both states B and C, as expected in the case that the enthalpy and entropy are constant with temperature. In this case, the slope of the line is $-\Delta H_{Ai}/R$, while the y-intercept is $\Delta S_{Ai}/R$, where $\Delta H_{Ai} = H_i - H_A$ and $\Delta S_{Ai} = S_i - S_A$. Both the A to B and A to C transitions have positive (unfavorable) enthalpy changes and positive (favorable) entropy changes, consistent with a weakening of intramolecular contacts. $T\Delta S_{Ai}$ values were calculated at T = 313 K.

Nucleus	Temp (°C)	[pro-IL-18] (mM)	B_0 (MHz)	CPMG Relaxation time (ms)	ν_{CPMG} range (Hz)
^{15}N [26]	40	0.75	1000, 800, 600	40	25 – 1000 (20 values)
^{15}N	35	0.25	1000	35	29 – 1000 (23 values)
^{15}N	32.5	0.25	1000	35	29 – 1000 (20 values)
^{15}N	29	0.25	1000	30	33 – 1000 (23 values)
^{15}N	25	0.25	1000	30	33 – 1000 (20 values)
^{15}N (*U*-[^{15}N])	40	0.5	1000, 800	40	25 – 1000 (20 values)
^{15}N (*U*-[^{15}N], pH 6.0)	40	0.5	800	40	25 – 1000 (20 values)
^{1}HN [27,28]	40	0.75	1000, 800	20	50 – 2000 (17 values)
^{13}CO [29]	40	1.1	800	25	40 – 1000 (17 values)
Methyl ^{13}C CPMG [30]	40	0.75	1000, 800	40	25 – 2000 (20 values)
Methyl ^{1}H [31]	40	0.75	1000, 800	35	29 – 1943 (19 values)

Table S1: Acquisition parameters of CPMG datasets.

Nucleus	Temp (°C)	[pro-IL-18] (mM)	B_0 (MHz)	Relaxation time (ms)	Weak B_1 field (Hz)	Frequency range (ppm)
^{15}N [32]	40	0.75	800	500, 600	44.3, 19.2	106 – 132 (24, 45 values)
^{15}N	35	0.25	800	500	42.8	106 – 132 (24 values)
^{15}N	32.5	0.25	800	500	42.8	106 – 132 (24 values)
^{15}N	29	0.25	800	500	42.8	106 – 132 (24 values)
^{15}N	25	0.25	800	500	42.7	106 – 132 (24 values)
^{1}HN [17]	40	0.6	800	400	20.2	6.4 – 10.6 (70 values)
^{13}CO [33]	40	0.5	600	300	27.0	169 – 181 (30 values)
^{13}Cα	40	0.5	600	300	27.0	49.4 – 66.5 (42 values)

$^{13}C\beta$	40	1.1	600	200	27.0	24.7 – 46.7 (54 values)
$^{1}H\alpha$ [34]	40	1.1	600	200	25.1	3.25 – 6.05 (29 values)
Methyl ^{13}C [35]	40	0.6	800	350	27.4	9.7 – 28.3 (60 values)
Methyl ^{1}H [36]	40	0.6	1000	300	38.6	-1.14 – 1.36 (32 values)

Table S2: Acquisition parameters of CEST datasets.

Residue	$^{15}N\ \Delta\varpi_{AB}$ (ppm)	$^{15}N\ \Delta\varpi_{AC}$ (ppm)	$^{1}HN\ \Delta\varpi_{AB}$ (ppm)	$^{1}HN\ \Delta\varpi_{AC}$ (ppm)	$^{13}CO\ \Delta\varpi_{AB}$ (ppm)	$^{13}CO\ \Delta\varpi_{AC}$ (ppm)	$^{13}C\alpha\ \Delta\varpi_{AC}$ (ppm)	$^{13}C\beta\ \Delta\varpi_{AC}$ (ppm)	$^{1}H\alpha\ \Delta\varpi_{AC}$ (ppm)
11	1.10±0.30	0.45±0.10	-	-	-0.62±0.07	-0.05±0.09	-	-	-
13	-	-	-0.59±0.03	-0.24±0.01	-	-	-	-	-
14	-1.60±0.10	-1.40±0.09	-	-	-	-	-	-	-
16	-	-	0.29±0.01	0.32±0.00	0.33±0.10	0.52±0.09	-	-	-
17	-	-	0.15±0.02	0.14±0.01	-	-	-	-	-
18	-1.50±0.10	-1.20±0.09	0.18±0.01	-0.00±0.03	-0.67±0.08	-0.61±0.09	-	-	-
19	-0.89±0.20	-0.76±0.10	0.18±0.01	0.12±0.00	0.35±0.10	0.52±0.10	-	-	-
22	-	-	-	-	-1.00±0.10	0.29±0.30	-	-	-
23	1.10±0.20	0.82±0.20	0.22±0.02	0.35±0.01	-	-	-	-	-
45	-	-	-	-	0.28±0.10	-0.70±0.05	-	-	-
46	1.10±0.09	0.29±0.05	0.27±0.01	0.10±0.00	1.00±0.05	-0.08±0.10	-2.10±0.40	-	-0.53±0.02
47	-	-	0.06±0.01	0.11±0.00	-1.10±0.20	0.32±0.40	-	-	-
48	-1.20±0.20	1.30±0.09	0.15±0.02	0.07±0.01	-1.30±0.20	-0.52±0.20	1.70±0.30	-	-
49	-1.90±0.20	-2.70±0.08	0.21±0.00	-0.17±0.00	-1.20±0.10	-2.00±0.10	-	-	-
50	-2.00±0.10	-1.70±0.07	-0.45±0.01	-0.23±0.00	-	-	-	-	-
51	-2.00±0.08	0.13±0.05	0.93±0.02	0.72±0.00	-	-	-	-	-
53	4.10±0.20	5.40±0.07	-0.13±0.01	-0.23±0.00	-	-	-2.20±0.20	-	-
54	5.40±0.30	7.30±0.08	0.43±0.02	0.97±0.01	1.10±0.07	1.30±0.08	-	-	-
55	-3.20±0.10	0.06±0.07	0.31±0.01	0.39±0.00	-0.57±0.08	-1.20±0.08	-	-	-
56	-1.40±0.10	-3.80±0.05	-0.22±0.01	-0.46±0.00	0.87±0.04	1.40±0.04	2.30±0.20	-1.40±0.30	-
57	-3.80±0.20	4.80±0.07	-0.18±0.01	0.85±0.00	1.90±0.50	-3.00±0.30	-	2.50±0.60	-
58	0.80±0.20	2.90±0.10	-0.25±0.01	-0.78±0.00	0.30±0.20	0.65±0.10	1.10±0.50	-1.80±0.80	-0.65±0.04
59	0.01±0.20	1.90±0.07	-0.09±0.03	0.49±0.00	-	-	-	-	-
60	-	-	-	-	-0.30±0.20	-0.46±0.10	-1.90±0.20	-	-
61	1.20±0.20	0.54±0.10	-	-	0.10±0.20	0.43±0.08	-	-	-
62	-0.62±0.10	-1.10±0.06	0.36±0.02	0.02±0.01	-	-	-	-	-
63	-0.32±0.10	-1.20±0.05	-0.18±0.01	0.13±0.01	-	-	-	-	-
64	-	-	-	-	-0.30±0.10	-0.41±0.06	-	-	-
66	-0.86±0.10	-1.10±0.07	-	-	-	-	-	-	-
81	1.30±0.10	0.24±0.08	-	-	-0.83±0.06	0.13±0.20	-	-	-
82	-2.40±0.10	-2.90±0.07	-0.21±0.01	-0.16±0.01	-0.79±0.10	-0.17±0.10	-	-	-
83	-4.60±0.20	-0.17±0.10	-0.31±0.02	0.14±0.02	-1.30±0.07	-0.25±0.06	-	-	-
86	-	-	-0.11±0.02	0.18±0.00	-	-	-	-	-
96	-0.70±0.30	-0.84±0.20	-0.09±0.07	-0.11±0.04	-	-	-	-	-
99	1.40±0.20	0.60±0.10	-	-	-	-	-	-	-
100	0.78±0.30	0.49±0.10	-	-	-	-	-	-	-
103	1.20±0.10	0.31±0.06	0.24±0.01	-0.22±0.01	-	-	-	-	-
104	-	-	-0.15±0.01	0.11±0.01	-	-	-	-	-
109	-	-	0.17±0.01	-0.02±0.03	-1.10±0.06	-0.03±0.07	-	-	-
118	-	-	-	-	-0.98±0.04	0.19±0.10	-	-	-
128	1.90±0.20	1.40±0.20	-	-	-	-	-	-	-
139	-	-	0.21±0.01	-0.15±0.01	-	-	-	-	-
149	1.10±0.20	0.46±0.10	-0.04±0.02	0.14±0.00	-	-	-	-	-
157	-	-	-	-	-0.80±0.10	-0.01±0.20	-	-	-
171	0.91±0.30	1.40±0.20	-	-	-	-	-	-	-
187	-	-	-	-	-0.04±0.08	-0.76±0.05	-	-	-
188	-	-	0.20±0.01	0.12±0.00	-1.30±0.08	-0.23±0.08	-	-	-

189	-	-	0.12±0.02	0.16±0.01	-	-	-	-	-
190	-	-	-0.20±0.01	-0.56±0.00	-0.48±0.10	-0.54±0.10	-	-	-
191	1.50±0.09	0.33±0.06	-	-	-	-	-	-	-
192	-	-	0.24±0.01	0.15±0.00	-	-	-	-	-

Table S3: Chemical shift differences between ground (A) and excited (B,C) states ($\Delta\varpi_{AX} = \varpi_X - \varpi_A$) for backbone and Cβ nuclei. '–' indicates negligibly small Δϖ or data that could not be fit due to peak overlap.

Residue	Random Coil GS	Random Coil ES	Beta Strand GS	Beta Strand ES
L45	32.5%	31.6%	66.9%	65.0%
S46	12.0%	22.9%	87.5%	75.6%
V47	28.4%	20.8%	71.6%	77.8%
I48	12.8%	13.4%	87.1%	86.5%
R49	47.3%	55.9%	50.4%	40.7%
N50	69.5%	68.3%	17.7%	22.1%
L51	69.6%	67.8%	6.0%	8.5%
N52	**43.9%**	**71.9%**	1.2%	4.4%
D53	**51.7%**	**76.4%**	2.3%	4.9%
Q54	**72.1%**	**48.4%**	**18.6%**	**48.8%**
V55	21.1%	22.2%	78.4%	76.9%
L56	6.7%	4.8%	93.2%	95.2%
F57	5.0%	11.1%	95.0%	88.5%
I58	15.9%	10.0%	82.2%	89.9%

Table S4: Secondary structure populations from *CheSPI* reveal only subtle changes between ground (GS) and excited (ES) states. Random coil and beta strand populations from *CheSPI* are shown for ground and excited (state C) states. In general, only small differences (≤~10%) are seen between the two states, including all the residues in β1 (45-48) and β* (55-58). Thus, the chemical shifts strongly suggest that these regions retain their secondary structure in the excited state. Populations changing by >20% are shown in bold, underlined font. These include a sizeable shift from random coil to beta strand for Q54, as well as shifts from turn to random coil for N52 and D53.

(A) Fit to linear model, $A \overset{1600\ s^{-1}}{\longleftrightarrow} \underset{0.53\%}{B} \overset{1330\ s^{-1}}{\longleftrightarrow} \underset{0.69\%}{C}$

Methyl	$^{13}C\ \Delta\varpi_{AB}$ (ppm)	$^{13}C\ \Delta\varpi_{AC}$ (ppm)	$^{1}H\ \Delta\varpi_{AB}$ (ppm)	$^{1}H\ \Delta\varpi_{AC}$ (ppm)
I11δ1	0.45±0.02	0.24±0.01	-0.09±0.00	0.02±0.01
L23δ1	0.22±0.20	-0.32±0.06	-0.21±0.00	-0.18±0.00
L23δ2	-1.00±0.03	-0.09±0.02	0.19±0.00	0.06±0.00
L51δ1	-0.63±0.02	-0.14±0.01	-0.14±0.00	-0.11±0.00
L51δ2	0.94±0.01	-0.02±0.01	-0.13±0.00	-0.07±0.00
V55γ1	-0.81±0.03	0.36±0.03	0.16±0.00	0.30±0.00
V55γ2	1.40±0.03	-2.30±0.04	-0.07±0.01	0.10±0.00
L56δ1	0.70±0.02	-0.11±0.03	0.13±0.00	0.17±0.00
L56δ2	0.87±0.02	2.20±0.01	-0.10±0.00	-0.13±0.00
I58δ1	-0.70±0.04	0.29±0.04	0.12±0.00	0.21±0.00
L65δ1	0.43±0.01	0.14±0.01	-0.07±0.00	-0.14±0.00
L65δ2	-0.51±0.04	0.28±0.02	0.14±0.00	0.06±0.00
I82δ1	0.79±0.02	0.32±0.01	-0.08±0.00	-0.22±0.00
I85δ1	-2.00±0.04	-0.59±0.01	0.23±0.00	0.35±0.00
V102γ1	-1.00±0.04	0.33±0.03	-0.17±0.00	-0.11±0.00
L110δ1	0.59±0.02	0.03±0.04	0.05±0.01	-0.09±0.00
I136δ1	0.49±0.05	0.19±0.03	0.10±0.01	-0.03±0.01
L172δ1	0.47±0.03	0.26±0.02	-0.10±0.01	0.02±0.01
L172δ2	0.85±0.04	-0.02±0.06	0.12±0.01	-0.09±0.01

(B) Fit to bifurcated model, $\underset{1.15\%}{E} \overset{800\ s^{-1}}{\longleftrightarrow} A \overset{460\ s^{-1}}{\longleftrightarrow} \underset{0.24\%}{D}$

Methyl	$^{13}C\ \Delta\varpi_{AE}$ (ppm)	$^{13}C\ \Delta\varpi_{AD}$ (ppm)	$^{1}H\ \Delta\varpi_{AE}$ (ppm)	$^{1}H\ \Delta\varpi_{AD}$ (ppm)
L45δ1	-0.20±0.01	-1.30±0.08	0.04±0.00	0.65±0.01
L45δ2	-0.28±0.01	1.60±0.06	0.04±0.00	0.43±0.01
V47γ1	0.43±0.01	1.50±0.07	-0.04±0.00	0.53±0.02
V47γ2	-0.25±0.01	0.11±0.20	0.05±0.00	0.60±0.04
I48δ1	-0.45±0.02	-1.40±0.04	0.11±0.00	-0.12±0.01

(C) Fit to V189 model, $A \overset{1400\ s^{-1}}{\longleftrightarrow} \underset{0.98\%}{ES1} \overset{5100\ s^{-1}}{\longleftrightarrow} \underset{1.50\%}{ES2}$

Methyl	$^{13}C\ \Delta\varpi_{A,ES1}$ (ppm)	$^{13}C\ \Delta\varpi_{A,ES2}$ (ppm)	$^{1}H\ \Delta\varpi_{A,ES1}$ (ppm)	$^{1}H\ \Delta\varpi_{A,ES2}$ (ppm)
V189γ1	-0.46±0.05	0.09±0.05	-0.21±0.01	0.23±0.01

Table S5: Chemical shift differences between ground (A) and excited (D/E for β1, ES1/ES2 for V189, B/C for all other methyls) states for ILV methyl ^{13}C and ^{1}H nuclei ($\Delta\varpi_{AX} = \varpi_X - \varpi_A$).

(A) Fit to bifurcated model, $\underset{1.15\%}{E} \overset{800\ s^{-1}}{\longleftrightarrow} A \overset{460\ s^{-1}}{\longleftrightarrow} \underset{0.24\%}{D}$

Residue	GS (g+/trans/g-)	State D (g+/trans/g-)	State E (g+/trans/g-)
L45	**46/54/0**	**75/25/0**	45/55/0
V47	**42/53/5**	**3/94/3**	31/59/10
I48	**0/93/7**	**0/67/33**	0/84/16

(B) Fit to linear model, $A \overset{1600\ s^{-1}}{\longleftrightarrow} \underset{0.53\%}{B} \overset{1330\ s^{-1}}{\longleftrightarrow} \underset{0.69\%}{C}$

Residue	GS (g+/trans/g-)	State C (g+/trans/g-)	State B (g+/trans/g-)
V55	**0/98/2**	**1/50/49**	**24/76/0**
L56	49/51/0	66/34/0	51/49/0
I58	0/64/36	0/69/31	0/51/49

Table S6: Rotamer populations determined from methyl ^{13}C chemical shifts show sizeable changes in excited state C/D, particularly for β1. Populations of *gauche*(+), *trans*, and *gauche*(-) rotamers are shown for Ile (χ2), Leu (χ2), and Val (χ1) residues in β1 and β* in ground (GS) and excited states. Populations which shift by >20% are shown in bold, underlined font, and include all three ILV residues in β1. Notably, I48 shifts from almost entirely *trans* in the ground state, to 2:1 *trans*:*gauche*(-) in the excited state (D), suggesting a loosening of the packing around this sidechain. Similarly, the nearby sidechain of V55 shows an even more pronounced shift from ~100% *trans* to 1:1 *trans*:*gauche*(-) (state C).

Excited State	Residues	Probes	Structural features
B	All exchanging (global)	All backbone, all sidechain methyls (19 of 25 methyl groups) except those from β1 (5 methyl groups) and V189γ1 in β13	β1 and β* retain secondary structure (Table S4). Enthalpic and entropic changes are consistent with reduction in interactions relative to states A and C (Figure S6). The rotamer populations of V55, that is proximal to I48, indicate lessening of restriction around I48 compared to state A (Table S6).
C	All exchanging (global)	All backbone, all sidechain methyls (19 of 25 methyl groups) except those from β1 (5 methyl groups) and V189γ1 in β13	β1 and β* retain secondary structure (Table S4). Enthalpic and entropic changes are consistent with reduction in packing relative to state A (Figure S6), and more loosening of structure around I48 than in state B, as reported by the sidechain rotamer populations of proximal residue V55 (Table S6).
D	β1 (local)	β1 sidechain methyls (L45, V47, I48)	This very lowly populated state (~0.25%), only detected via relaxation data of the β1 sidechain methyl groups, shows loosening in structure around I48 based on the I48 rotamer populations (Table S6). As the β1 sidechain methyl data could be comparably fit with a D↔A↔B↔C model (relative to the E↔A↔D model), where states A, B, and C are obtained from fits of the backbone data, state D could simply be an additional state for the β1 methyls (*i.e.*, a slightly more complex exchange model encompassing the exchange process characterized for all other relaxation data).
E	β1 (local)	β1 sidechain methyls (L45, V47, I48)	Generally small chemical shift differences (Table S5) suggest little deviation from the ground state structure in this region, with similar packing of I48 as in state A. As the β1 sidechain methyl data could be comparably fit with a D↔A↔B↔C model (relative to E↔A↔D model), it is possible that state E in fact represents a 'composite' of

			states B and C, though the data are insufficient to prove this.

Table S7: Structural description of excited states that are formed via µs-ms timescale dynamics. These states are formed via two distinct processes that can be described via 3-site chemical exchange, $\boldsymbol{A \overset{1600\ s^{-1}}{\Longleftrightarrow} B_{0.53\%} \overset{1330\ s^{-1}}{\Longleftrightarrow} C_{0.69\%}}$ **(19 of 25 methyl group probes; Figure 6c) and** $\boldsymbol{E_{1.15\%} \overset{800\ s^{-1}}{\Longleftrightarrow} A \overset{460\ s^{-1}}{\Longleftrightarrow} D_{0.24\%}}$ **(5 of 25 methyls; Figure 6c).**

Residue	$\Delta G\left(\frac{kcal}{mol}\right)$	Residue	$\Delta G\left(\frac{kcal}{mol}\right)$	Residue	$\Delta G\left(\frac{kcal}{mol}\right)$	Residue	$\Delta G\left(\frac{kcal}{mol}\right)$
2	ND (fast)	**53**	ND (fast)	**106**	ND (fast)	**167**	ND (fast)
3	ND (fast)	**54**	2.68±0.02	**107**	ND (fast)	**168**	7.10±0.04
4	ND (fast)	**55**	2.47±0.01	**108**	6.85±0.20	**169**	1.99±0.01
6	ND (fast)	**56**	2.25±0.01	**109**	ND (slow)	**170**	6.87±0.80
7	ND (fast)	**57**	2.32±0.01	**110**	ND (slow)	**171**	ND (slow)
8	ND (fast)	**59**	ND (fast)	**112**	8.65±0.30	**173**	ND (slow)
9	ND (fast)	**60**	ND (fast)	**113**	3.93±0.03	**174**	5.18±0.01
10	5.99±0.02	**61**	ND (fast)	**114**	ND (fast)	**175**	ND (slow)
12	3.68±0.01	**62**	ND (fast)	**115**	4.80±0.06	**176**	3.12±0.01
13	5.89±0.01	**63**	ND (fast)	**117**	2.55±0.02	**177**	3.36±0.01
14	5.34±0.02	**65**	ND (fast)	**118**	ND (slow)	**178**	ND (fast)
15	6.20±0.01	**66**	ND (fast)	**119**	3.26±0.03	**179**	4.46±0.01
16	4.60±0.01	**67**	ND (fast)	**120**	6.23±0.02	**180**	ND (fast)
17	6.46±0.03	**68**	ND (fast)	**121**	ND (fast)	**181**	ND (fast)
18	ND (fast)	**69**	ND (fast)	**122**	3.05±0.02	**182**	ND (fast)
19	5.06±0.02	**70**	ND (fast)	**123**	ND (fast)	**183**	ND (fast)
20	ND (fast)	**71**	ND (fast)	**126**	ND (fast)	**184**	ND (fast)
21	ND (fast)	**72**	ND (fast)	**127**	ND (fast)	**185**	3.34±0.04
22	5.69±0.00	**73**	ND (fast)	**128**	ND (fast)	**186**	4.34±0.01
23	5.91±0.05	**74**	ND (fast)	**129**	ND (fast)	**187**	6.76±0.20
24	5.79±0.03	**75**	ND (fast)	**130**	ND (fast)	**188**	6.77±0.04
25	6.10±0.02	**76**	ND (fast)	**131**	ND (fast)	**190**	4.66±0.03
26	5.75±0.04	**77**	ND (fast)	**132**	ND (fast)	**191**	3.50±0.04
27	3.85±0.03	**78**	ND (fast)	**133**	ND (fast)	**192**	ND (fast)
28	3.23±0.01	**80**	ND (fast)	**137**	ND (slow)	**193**	ND (fast)
29	ND (fast)	**81**	ND (fast)	**138**	ND (slow)		
30	ND (fast)	**82**	ND (slow)	**139**	6.85±0.10		
31	ND (fast)	**83**	ND (slow)	**140**	ND (slow)		
32	ND (fast)	**84**	ND (slow)	**144**	ND (fast)		
33	ND (fast)	**85**	ND (slow)	**145**	ND (fast)		
34	ND (fast)	**86**	6.76±0.06	**146**	ND (fast)		
35	ND (fast)	**87**	5.41±0.04	**147**	ND (fast)		
36	ND (fast)	**88**	4.61±0.06	**148**	ND (fast)		
37	ND (fast)	**89**	ND (fast)	**149**	ND (fast)		
38	ND (fast)	**90**	ND (fast)	**151**	ND (slow)		
39	ND (fast)	**91**	ND (fast)	**152**	ND (slow)		
40	ND (fast)	**92**	ND (fast)	**153**	ND (slow)		
41	ND (fast)	**94**	ND (fast)	**154**	ND (slow)		
42	ND (fast)	**95**	ND (fast)	**155**	ND (fast)		
43	ND (fast)	**96**	ND (fast)	**156**	5.52±0.01		
44	ND (fast)	**97**	5.71±0.02	**157**	2.88±0.02		
45	2.94±0.01	**98**	ND (slow)	**158**	3.96±0.04		
46	3.65±0.01	**99**	ND (slow)	**159**	ND (slow)		
47	2.93±0.01	**100**	ND (slow)	**160**	ND (slow)		
48	3.03±0.07	**101**	ND (slow)	**162**	ND (slow)		
49	3.35±0.02	**102**	ND (slow)	**163**	ND (slow)		
50	ND (fast)	**103**	ND (slow)	**164**	ND (slow)		
51	ND (fast)	**104**	4.18±0.01	**165**	ND (fast)		
52	ND (fast)	**105**	ND (fast)	**166**	ND (fast)		

Table S8: Local unfolding ΔG values from HDX. Residues listed as ND (fast) are those whose amide signal had already fully decayed at the first time point. Those listed as ND (slow) showed

very little signal loss during the course of the measurements, such that a decay rate could not be reliably fit.

(A) Fit to linear model

Probe[a]	p_B (%)	p_C (%)	$k_{ex,AB}$ (s^{-1})	$k_{ex,BC}$ (s^{-1})	$k_{ex,AC}$ (s^{-1})
^{15}N & ILV methyls (40 ˚C, ^{2}H)[b]	0.53±0.01	0.69±0.02	1600±80	1330±50	0 (fixed)
^{15}N (35 ˚C, ^{2}H)	0.36±0.02	0.58±0.06	1600±200	1200±200	0 (fixed)
^{15}N (32.5 ˚C, ^{2}H)	0.33±0.01	0.51±0.04	1600±200	1100±200	0 (fixed)
^{15}N (29 ˚C, ^{2}H)	0.25±0.00	0.42±0.01	1100±40	1120±50	0 (fixed)
^{15}N (25 ˚C, ^{2}H)	0.20±0.00	0.38±0.01	900±40	1120 (fixed)	0 (fixed)
^{15}N (40 ˚C, ^{1}H)[c]	0.47±0.01	0.51±0.03	1220±30	1290±40	0 (fixed)
^{15}N (40 ˚C, ^{1}H, pH 6.0)	0.54±0.02	0.42±0.06	1000±60	1500±100	0 (fixed)

(B) Fit to bifurcated model

Probe[a]	p_E (%)	p_D (%)	$k_{ex,AE}$ (s^{-1})	$k_{ex,DE}$ (s^{-1})	$k_{ex,AD}$ (s^{-1})
β1 methyl groups (L45, V47, I48)	1.15±0.03	0.24±0.01	800±20	0 (fixed)	460±20

(C) Fit to V189 model

Probe[a]	p_{ES1} (%)	p_{ES2} (%)	$k_{ex,AES2}$ (s^{-1})	$k_{ex,ES1ES2}$ (s^{-1})	$k_{ex,AES1}$ (s^{-1})
V189γ_1	0.98±0.04	1.50±0.10	0 (fixed)	5100±400	1400±100

Table S9: 3-state exchange model parameters.

[a]Unless explicitly indicated otherwise, pH = 6.5.

[b] ^{2}H refers to a *U*-[^{2}H,^{15}N] ILV $^{13}CH_3$ labeled (perdeuterated) sample. These parameters were used for the analysis of the ^{15}N, ^{1}HN, and methyl ^{13}C/^{1}H (except β1, V189γ_1) CPMG and CEST data at 40 ˚C.

[c] ^{1}H refers to a *U*-[^{15}N] labeled (fully protonated) sample. These parameters were used for the analysis of the ^{13}CO, ^{13}Cα, ^{13}Cβ, and ^{1}Hα (*U*-[^{13}C,^{15}N] labeling) CPMG/CEST data at 40 ˚C.

References

(1) Dong, Y.; Bonin, J. P.; Devant, P.; Liang, Z.; Sever, A. I. M.; Mintseris, J.; Aramini, J. M.; Du, G.; Gygi, S. P.; Kagan, J. C.; Kay, L. E.; Wu, H. Structural Transitions Enable Interleukin-18 Maturation and Signaling. *Immunity* **2024**, *57* (7), 1533-1548.e10. https://doi.org/10.1016/j.immuni.2024.04.015.

(2) Covington, A. K.; Paabo, Maya.; Robinson, R. Anthony.; Bates, R. G. Use of the Glass Electrode in Deuterium Oxide and the Relation between the Standardized PD (PaD) Scale and the Operational PH in Heavy Water. *Anal Chem* **1968**, *40* (4), 700–706. https://doi.org/10.1021/ac60260a013.

(3) Delaglio, F.; Grzesiek, S.; Vuister, GeertenW.; Zhu, G.; Pfeifer, J.; Bax, A. NMRPipe: A Multidimensional Spectral Processing System Based on UNIX Pipes. *J Biomol NMR* **1995**, *6* (3). https://doi.org/10.1007/BF00197809.

(4) Lee, W.; Tonelli, M.; Markley, J. L. NMRFAM-SPARKY: Enhanced Software for Biomolecular NMR Spectroscopy. *Bioinformatics* **2015**, *31* (8), 1325–1327. https://doi.org/10.1093/bioinformatics/btu830.

(5) Kay, L.; Keifer, P.; Saarinen, T. Pure Absorption Gradient Enhanced Heteronuclear Single Quantum Correlation Spectroscopy with Improved Sensitivity. *J Am Chem Soc* **1992**, *114* (26), 10663–10665. https://doi.org/10.1021/ja00052a088.

(6) Hansen, D. F.; Yang, D.; Feng, H.; Zhou, Z.; Wiesner, S.; Bai, Y.; Kay, L. E. An Exchange-Free Measure of ^{15}N Transverse Relaxation: An NMR Spectroscopy Application to the Study of a Folding Intermediate with Pervasive Chemical Exchange. *J Am Chem Soc* **2007**, *129* (37), 11468–11479. https://doi.org/10.1021/ja072717t.

(7) Ferrage, F.; Cowburn, D.; Ghose, R. Accurate Sampling of High-Frequency Motions in Proteins by Steady-State ^{15}N−{ ^{1}H} Nuclear Overhauser Effect Measurements in the Presence of Cross-Correlated Relaxation. *J Am Chem Soc* **2009**, *131* (17), 6048–6049. https://doi.org/10.1021/ja809526q.

(8) Farrow, N. A.; Muhandiram, R.; Singer, A. U.; Pascal, S. M.; Kay, C. M.; Gish, G.; Shoelson, S. E.; Pawson, T.; Forman-Kay, J. D.; Kay, L. E. Backbone Dynamics of a Free and a Phosphopeptide-Complexed Src Homology 2 Domain Studied by 15N NMR Relaxation. *Biochemistry* **1994**, *33* (19), 5984–6003. https://doi.org/10.1021/bi00185a040.

(9) Sun, H.; Kay, L. E.; Tugarinov, V. An Optimized Relaxation-Based Coherence Transfer NMR Experiment for the Measurement of Side-Chain Order in Methyl-Protonated, Highly Deuterated Proteins. *J Phys Chem B* **2011**, *115* (49), 14878–14884. https://doi.org/10.1021/jp209049k.

(10) Bolik-Coulon, N.; Hansen, D. F.; Kay, L. E. Optimizing Frequency Sampling in CEST Experiments. *J Biomol NMR* **2022**, *76* (5–6), 167–183. https://doi.org/10.1007/s10858-022-00403-2.

(11) Yuwen, T.; Kay, L. E. A New Class of CEST Experiment Based on Selecting Different Magnetization Components at the Start and End of the CEST Relaxation Element: An Application to 1H CEST. *J Biomol NMR* **2018**, *70* (2), 93–102. https://doi.org/10.1007/s10858-017-0161-2.

(12) Hansen, D. F.; Feng, H.; Zhou, Z.; Bai, Y.; Kay, L. E. Selective Characterization of Microsecond Motions in Proteins by NMR Relaxation. *J Am Chem Soc* **2009**, *131* (44), 16257–16265. https://doi.org/10.1021/ja906842s.

(13) Cavanagh, J.; Fairbrother, W.; Palmer, A.; Rance, M.; Skelton, N. *Protein NMR Spectroscopy*, 2nd ed.; Academic Press, 2007.

(14) Farrow, N. A.; Zhang, O.; Szabo, A.; Torchia, D. A.; Kay, L. E. Spectral Density Function Mapping Using 15N Relaxation Data Exclusively. *J Biomol NMR* **1995**, *6* (2), 153–162. https://doi.org/10.1007/BF00211779.

(15) Berlin, K.; Longhini, A.; Dayie, T. K.; Fushman, D. Deriving Quantitative Dynamics Information for Proteins and RNAs Using ROTDIF with a Graphical User Interface. *J Biomol NMR* **2013**, *57* (4), 333–352. https://doi.org/10.1007/s10858-013-9791-1.

(16) Mandel, A. M.; Akke, M.; Palmer, I. A. G. Backbone Dynamics of Ribonuclease HI: Correlations with Structure and Function in an Active Enzyme. *J Mol Biol* **1995**, *246* (1), 144–163. https://doi.org/10.1006/jmbi.1994.0073.

(17) Yuwen, T.; Sekhar, A.; Kay, L. E. Separating Dipolar and Chemical Exchange Magnetization Transfer Processes in ^{1}H-CEST. *Angewandte Chemie International Edition* **2017**, *56* (22), 6122–6125. https://doi.org/10.1002/anie.201610759.

(18) Ferraro, D. M.; Lazo, N. D.; Robertson, A. D. EX1 Hydrogen Exchange and Protein Folding. *Biochemistry* **2004**, *43* (3), 587–594. https://doi.org/10.1021/bi035943y.

(19) Nguyen, D.; Mayne, L.; Phillips, M. C.; Walter Englander, S. Reference Parameters for Protein Hydrogen Exchange Rates. *J Am Soc Mass Spectrom* **2018**, *29* (9), 1936–1939. https://doi.org/10.1007/s13361-018-2021-z.

(20) Connelly, G. P.; Bai, Y.; Jeng, M.; Englander, S. W. Isotope Effects in Peptide Group Hydrogen Exchange. *Proteins: Structure, Function, and Bioinformatics* **1993**, *17* (1), 87–92. https://doi.org/10.1002/prot.340170111.

(21) Bai, Y.; Milne, J. S.; Mayne, L.; Englander, S. W. Primary Structure Effects on Peptide Group Hydrogen Exchange. *Proteins: Structure, Function, and Bioinformatics* **1993**, *17* (1), 75–86. https://doi.org/10.1002/prot.340170110.

(22) Kjaergaard, M.; Poulsen, F. M. Sequence Correction of Random Coil Chemical Shifts: Correlation between Neighbor Correction Factors and Changes in the Ramachandran Distribution. *J Biomol NMR* **2011**, *50* (2), 157–165. https://doi.org/10.1007/s10858-011-9508-2.

(23) Kjaergaard, M.; Brander, S.; Poulsen, F. M. Random Coil Chemical Shift for Intrinsically Disordered Proteins: Effects of Temperature and PH. *J Biomol NMR* **2011**, *49* (2), 139–149. https://doi.org/10.1007/s10858-011-9472-x.

(24) Schwarzinger, S.; Kroon, G. J. A.; Foss, T. R.; Chung, J.; Wright, P. E.; Dyson, H. J. Sequence-Dependent Correction of Random Coil NMR Chemical Shifts. *J Am Chem Soc* **2001**, *123* (13), 2970–2978. https://doi.org/10.1021/ja003760i.

(25) Maltsev, A. S.; Ying, J.; Bax, A. Deuterium Isotope Shifts for Backbone 1H, 15N and 13C Nuclei in Intrinsically Disordered Protein α-Synuclein. *J Biomol NMR* **2012**, *54* (2), 181–191. https://doi.org/10.1007/s10858-012-9666-x.

(26) Hansen, D. F.; Vallurupalli, P.; Kay, L. E. An Improved ^{15}N Relaxation Dispersion Experiment for the Measurement of Millisecond Time-Scale Dynamics in Proteins. *J Phys Chem B* **2008**, *112* (19), 5898–5904. https://doi.org/10.1021/jp074793o.

(27) Ishima, R.; Torchia, D. A. Extending the Range of Amide Proton Relaxation Dispersion Experiments in Proteins Using a Constant-Time Relaxation-Compensated CPMG Approach. *J Biomol NMR* **2003**, *25* (3), 243–248. https://doi.org/10.1023/A:1022851228405.

(28) Yuwen, T.; Kay, L. E. Revisiting 1HN CPMG Relaxation Dispersion Experiments: A Simple Modification Can Eliminate Large Artifacts. *J Biomol NMR* **2019**, *73* (10–11), 641–650. https://doi.org/10.1007/s10858-019-00276-y.

(29) Lundström, P.; Hansen, D. F.; Kay, L. E. Measurement of Carbonyl Chemical Shifts of Excited Protein States by Relaxation Dispersion NMR Spectroscopy: Comparison between Uniformly and Selectively 13C Labeled Samples. *J Biomol NMR* **2008**, *42* (1), 35–47. https://doi.org/10.1007/s10858-008-9260-4.

(30) Korzhnev, D. M.; Kloiber, K.; Kanelis, V.; Tugarinov, V.; Kay, L. E. Probing Slow Dynamics in High Molecular Weight Proteins by Methyl-TROSY NMR Spectroscopy: Application to a 723-Residue Enzyme. *J Am Chem Soc* **2004**, *126* (12), 3964–3973. https://doi.org/10.1021/ja039587i.

(31) Yuwen, T.; Huang, R.; Vallurupalli, P.; Kay, L. E. A Methyl-TROSY-Based ^{1}H Relaxation Dispersion Experiment for Studies of Conformational Exchange in High Molecular Weight Proteins. *Angewandte Chemie International Edition* **2019**, *58* (19), 6250–6254. https://doi.org/10.1002/anie.201900241.

(32) Vallurupalli, P.; Bouvignies, G.; Kay, L. E. Studying "Invisible" Excited Protein States in Slow Exchange with a Major State Conformation. *J Am Chem Soc* **2012**, *134* (19), 8148–8161. https://doi.org/10.1021/ja3001419.

(33) Vallurupalli, P.; Kay, L. E. Probing Slow Chemical Exchange at Carbonyl Sites in Proteins by Chemical Exchange Saturation Transfer NMR Spectroscopy. *Angewandte Chemie International Edition* **2013**, *52* (15), 4156–4159. https://doi.org/10.1002/anie.201209118.

(34) Kumar, A.; Madhurima, K.; Naganathan, A. N.; Vallurupalli, P.; Sekhar, A. Probing Excited State 1Hα Chemical Shifts in Intrinsically Disordered Proteins with a Triple Resonance-Based CEST Experiment: Application to a Disorder-to-Order Switch. *Methods* **2023**, *218*, 198–209. https://doi.org/10.1016/j.ymeth.2023.08.009.

(35) Bouvignies, G.; Kay, L. E. A 2D 13C-CEST Experiment for Studying Slowly Exchanging Protein Systems Using Methyl Probes: An Application to Protein Folding. *J Biomol NMR* **2012**, *53* (4), 303–310. https://doi.org/10.1007/s10858-012-9640-7.

(36) Yuwen, T.; Huang, R.; Kay, L. E. Probing Slow Timescale Dynamics in Proteins Using Methyl 1H CEST. *J Biomol NMR* **2017**, *68* (3), 215–224. https://doi.org/10.1007/s10858-017-0121-x.